SCIENTIFIC REPORTS

OPEN

SUBJECT AREAS:
SUPERCONDUCTING PROPERTIES AND MATERIALS
SURFACES, INTERFACES AND THIN FILMS

Received
15 May 2014

Accepted
13 August 2014

Published
1 September 2014

Correspondence and requests for materials should be addressed to E.S. (evelyn.stilp@psi.ch)

Controlling the near-surface superfluid density in underdoped $YBa_2Cu_3O_{6+x}$ by photo-illumination

E. Stilp[1,2], A. Suter[1], T. Prokscha[1], Z. Salman[1], E. Morenzoni[1], H. Keller[2], P. Pahlke[3,4], R. Hühne[4], C. Bernhard[5], Ruixing Liang[6,7], W. N. Hardy[6,7], D. A. Bonn[6,7], J. C. Baglo[6] & R. F. Kiefl[6]

[1]Laboratory for Muon Spin Spectroscopy, Paul Scherrer Institut, CH-5232 Villigen PSI, Switzerland, [2]Physik-Institut der Universität Zürich, Winterthurerstrasse 190, CH-8057 Zürich, Switzerland, [3]Institut für Festkörperphysik, Technische Universität Dresden, D-01062 Dresden, Germany, [4]Institute for Metallic Materials, IFW Dresden, D-01069 Dresden, Germany, [5]Department of Physics, University of Fribourg, CH-1700 Fribourg, Switzerland, [6]Department of Physics and Astronomy, University of British Columbia, Vancouver, British Columbia, Canada V6T 1Z1, [7]Canadian Institute for Advanced Research, Toronto, Ontario, Canada M5G 1Z8.

The interaction with light weakens the superconducting ground state in classical superconductors. The situation in cuprate superconductors is more complicated: illumination increases the charge carrier density, a photo-induced effect that persists below room temperature. Furthermore, systematic investigations in underdoped $YBa_2Cu_3O_{6+x}$ (YBCO) have shown an enhanced critical temperature T_c. Until now, studies of photo-persistent conductivity (PPC) have been limited to investigations of structural and transport properties, as well as the onset of superconductivity. Here we show how changes in the magnetic screening profile of YBCO in the Meissner state due to PPC can be determined on a nanometer scale utilizing low-energy muons. The data obtained reveal a strongly increased superfluid density within the first few tens of nanometers from the sample surface. Our findings suggest a non-trivial modification of the near-surface band structure and give direct evidence that the superfluid density of YBCO can be controlled by light illumination.

Tuning the superfluid density of cuprate systems without introducing additional disorder into the structure is challenging. Illumination with photons is one tool to realize this. Photo-persistent conductivity caused by visible light is widely known in semiconductors such as doping-modulated superlattices of hydrogenated amorphous silicon (a-Si:H)[1] or in low doped n-type Ge[2]. In these systems the recombination is inhibited by the spatial separation of electrons and holes, leading to long recombination lifetimes. In conventional superconductors, short-time illumination with photons having energies larger than the Cooper pair binding energy causes transient pair breaking, leading to the creation of quasiparticles[3]. In this case, illumination reduces the energy gap and therefore weakens superconductivity. In contrast, in cuprates it has been demonstrated that mid-infrared femtosecond pulses induce transient superconductivity[4].

Remarkably, studies on $YBa_2Cu_3O_{6+x}$ with reduced oxygen content ($x < 1$) show a persistent increase in the electrical conductivity after continuous illumination with visible light, in thin films[5,6] as well as in single crystals[7]. The critical temperature T_c is shifted to higher values for a broad range of oxygen concentrations ($0.4 \leq x \leq 0.9$) up to $\Delta T_{c,max} = 15$ K[8]. The magnitude of the shift strongly depends on the oxygen content x, the temperature at which the illumination is performed, and the photon dose[8]. YBCO samples with $x < 0.4$, which are close to the metal-insulator transition, even become superconducting under illumination[9]. The photo-induced effects are only present for photon energies higher than 1.6 eV. The changes in resistivity and T_c persist until the temperature is raised beyond 270 K. Accordingly, in the literature the effect is referred to as photo-persistent conductivity. Above 270 K the resistivity relaxes back on time scales of hours to days, depending on the temperature[9]. This time scale is similar to that required for YBCO samples to stabilize their properties at room temperature after deoxygenation of the sample at high temperatures[10]. The PPC is fully reversible and reproducible. If infrared (IR) light is used for illumination an increase in conductivity is observed as well, but with a much smaller magnitude[11]. But if IR illumination is performed after illumination with visible light, the PPC is reduced by about 2 – 10% even at low temperatures.

Different origins have been proposed to explain the PPC, which can be generally divided into two main lines: (a) Photo-induced charge transfer and (b) photo-assisted oxygen ordering. The underlying mechanisms can only

be understood by taking into account the anisotropic structure of YBCO. In contrast to most other cuprate systems, YBCO consists of CuO_2 planes separated by CuO_x layers which form Cu-O chains along the crystallographic b axis at higher doping levels x (Fig. 1). At low x the oxygen atoms in these CuO_x layers are isolated from each other[9]. Longer Cu-O chains form at higher x, leading to the formation of localized holes in the CuO_x layers. This results in a charge transfer of electrons from the CuO_2 planes to the Cu-O chains increasing the number of mobile holes in the CuO_2 planes. Therefore, the ordering of oxygen in the CuO_x layers plays a major role for conductivity as well as for superconductivity in YBCO. A longer average chain length leads to a higher charge carrier density in the CuO_2 planes and to a higher T_c[12] on the underdoped side of the phase diagram.

The scenario discussed above is crucial to an understanding of the proposed PPC mechanisms. In the case of photo-induced charge transfer, the absorbed photons create electron-hole pairs. The electrons are trapped at defects such as oxygen vacancies, preventing recombination. The holes are transfered to the CuO_2 planes where they contribute to the conductivity and, at low temperatures to the superconductivity. Thus mechanism (a) explains the increase in conductivity and the shift in T_c. However, it does not provide a natural explanation for the effects of IR light[11]. The photo-assisted oxygen ordering mechanism (b) assumes that the photons initiate a reordering of oxygen in the CuO_x layers, so that longer Cu-O chain fragments are present. This leads to an enhanced charge carrier transfer to the CuO_2 planes where superconductivity takes place. The proposed mechanism agrees with the observation that the time dependence of the resistivity relaxation is similar for photo-induced changes and for oxygen reordering after annealing. However, mechanism (b) alone fails to explain the IR experiments and why the oxygen atoms move under illumination. Therefore, a combination of both mechanisms was proposed[11].

In the combined model the trapped electrons at the oxygen vacancies act as local perturbations that modify the local electric field distribution. The induced dipole moments cause the movement of the oxygen in the CuO_x layers, resulting in a lengthening of the chain fragments. A simplified theoretical model[13] agrees with this interpretation. It confirms that local perturbations can affect the average chain length. Experimental[14] as well as theoretical[15] investigations have also shown that electrical fields influence the oxygen ordering and change T_c. The combined mechanism accounts for the infrared quenching, predicts the correct time dependence of the photo-excitation process, and gives the correct scale of the changes in resistivity produced by illumination.

Even though extensive structural studies were able to correlate the chain ordering to the charge transfer, leading to changes of the resistivity and T_c, little is known how illumination affects the superconducting state on the microscopic level. In our study we focused on a detailed investigation of the magnetic screening profile $B(z)$ in the Meissner state, utilizing low-energy muon spin rotation (LE-μSR)[16,17].

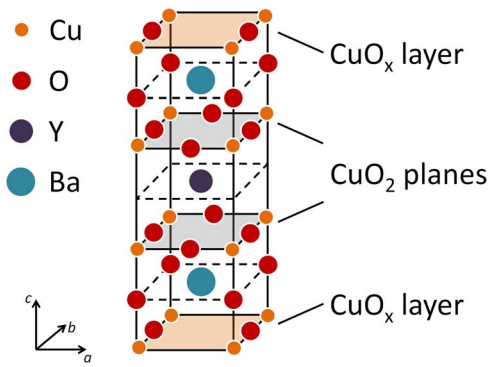

Figure 1 | The crystal structure of $YBa_2Cu_3O_{6+x}$.

Results & Discussion

LE-μSR is an unique and powerful technique to measure non-trivial $B(z)$ on a nanometer scale in a wide variety of superconducting single crystals[18], thin films[19,20], and heterostructures[21,22], allowing also the observation of non-local effects[23–25]. Positively charged muons are slowed down and implanted into the samples at different mean implantation depths $\bar{z}$ (Figs. 2 and 3). The Larmor frequency of the muons, $\omega_L(z)$, directly related to the local magnetic field B at the muon stopping site ($\omega_L = \gamma_\mu B$ with the muon gyromagnetic moment $\gamma_\mu = 2\pi \cdot 135.5$ MHz/T), is measured via the decay positron. For a semi-infinite sample, the London equation

$$\frac{d^2B(z)}{dz^2} = \frac{1}{\lambda_L^2}B(z), \tag{1}$$

yields a magnetic penetration profile $B(z) = B_{ext} \cdot \exp(-z/\lambda_L)$, for the boundary condition $B(z = 0) = B_{ext}$. Therefore, measuring $B(z)$ allows one to determine the magnetic penetration depth λ_L and thereby the superfluid density $n_s \propto 1/\lambda_L^2$ [26]. The process cycle and the conditions of the LE-μSR measurements are presented schematically in Fig. 3. The in-situ illumination setup is described in detail in the supplementary section S1.

Two sets of YBCO thin films ($x = 0.42, 0.67$) with twinned crystallographic a and b axes were investigated along with a detwinned single-crystal mosaic ($x = 0.67$). The YBCO thin film sets show shifts of $\Delta T_c = 6.4(6)$ K ($x = 0.42$) and $\Delta T_c = 0.9(1)$ K ($x = 0.67$) after illumination with about $7 \cdot 10^{22}$ photons/cm^2, in agreement with previous results[8] (see Fig. 4). The magnetic screening profiles $\bar{B}(\bar{z})$ determined by LE-μSR show for the initial state (before illumination) an exponential decay for the single crystals and a cosh behaviour in the thin films (resulting from the exponential penetration of the magnetic field from both interfaces) as depicted in Fig. 2. After illumination, all magnetic screening profiles are shifted to lower values and exhibit a pronounced change in shape. The corresponding superfluid density n_s is enhanced in all sample sets investigated.

Two different scenarios for the PPC change of n_s as function of the depth z can be envisaged: (i) The additional charge carries are mobile along the lattice c direction, hence they are distributed homogeneously over the whole sample. The superfluid density is raised, but is still constant as a function of depth z. Thus only the absolute value of λ_L is changed. Since the additional superfluid density is spatially averaged over the volume in scenario (i), the PPC changes of n_s would be much less pronounced or more likely to be absent in single crystals compared to thin films. However, this does not account for our results, since a change in $\bar{B}(\bar{z})$ is observed in the YBCO ortho-VIII single crystals (see Fig. 2c). (ii) The PPC charge carriers are pinned to the layer where they are created. Here, the changes in the superfluid density would be proportional to the light penetration profile: n_s increases mainly close to the vacuum interface, since the light penetrates exponentially into the sample. A depth-dependent superfluid density leads in turn to a modification of the Meissner screening field profile $B(z)$. Our results agree with the second scenario. At small depths z the applied magnetic field is more strongly shielded compared to the initial state. At higher z values the $B(z)$ curves are almost parallel. We therefore describe the penetration profiles of the illuminated samples by:

$$\frac{d^2B(z)}{dz^2} = \left(\frac{1}{\lambda_L^2} + \frac{1}{\lambda_P^2}e^{-z/\zeta}\right)B(z), \tag{2}$$

where $1/\lambda_L^2$ is proportional to the initial superfluid density before illumination $n_{s,0}$, $1/\lambda_P^2$ corresponds to the photo-induced superfluid density at the vacuum interface $n_{s,illum}$, and ζ is the characteristic

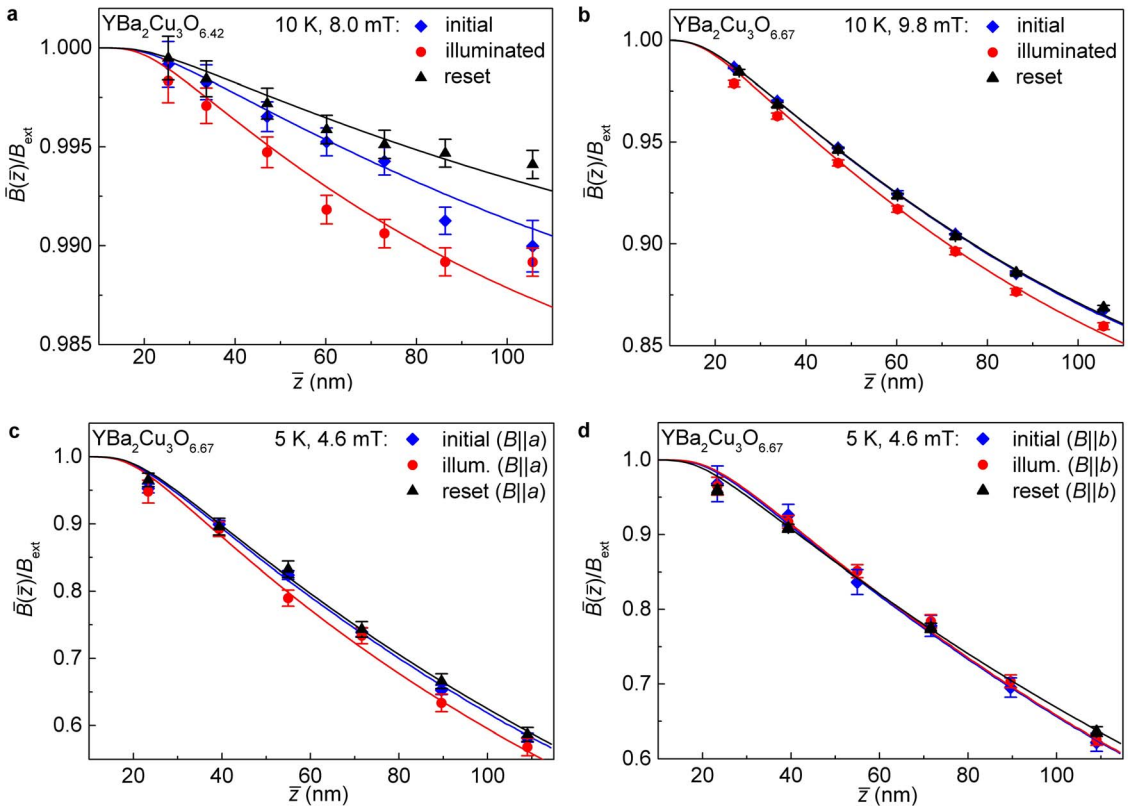

Figure 2 | Modifications of the magnetic screening profile due to illumination. The magnetic penetration profile $\bar{B}(\bar{z})$ along the crystallographic c axis normalized to the applied magnetic field B_{ext} of thin-film $YBa_2Cu_3O_{6.42}$ (**a**), thin-film $YBa_2Cu_3O_{6.67}$ (**b**), and detwinned $YBa_2Cu_3O_{6.67}$ single crystals in the ortho-VIII phase for B_{ext} applied parallel to the crystallographic a axis (**c**) and for B_{ext} parallel to the b axis (**d**). The applied magnetic field B_{ext} and the temperature are given in each figure. The presented field profiles correspond to the initial state (blue diamonds, before illumination), to the illuminated state (red circles, after illumination) and the recovered state (black triangles, after heating up to room temperature for about one day). The pronounced changes of the $\bar{B}(\bar{z})$ profiles (in magnitude and shape) due to visible light illumination are caused by a substantial increase of the superfluid density on the nanometer length scale to the vacuum interface.

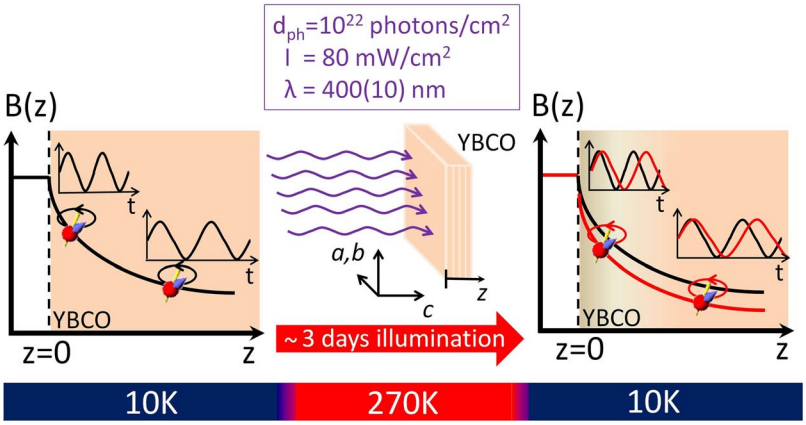

Figure 3 | Schematic diagram of the experimental μSR process cycle. Left panel: After zero field cooling (ZFC) the sample an external magnetic field $B_{ext}/\mu_0 < H_{c_1}$ was applied within the ab-plane. The interface to the vacuum is labeled with $z = 0$. The screened magnetic field values B at different depths z along the crystallographic c axis were determined via the Larmor frequency of the implanted positively charged muons (red circles) $\omega_L = \gamma_\mu B$ at 10 K for the YBCO thin films and at 5 K for the YBCO ortho-VIII single crystals. The muon spin precesses at ω_L around the local magnetic field B present in the sample. The Larmor frequency ω_L is extracted from the muon-spin polarization function $P(t)$ measured via the decay positron. Center panel: The LE-μSR measurements were followed by the in-situ photo illumination of the samples for $\sim$ 3 days ($4-5 \cdot 10^{22}$ photons/cm^2) at 270 K with a high-intensity LED source. Right panel: Afterwards the samples were ZFC to 10 K/5 K, repeating the measurement of the screened magnetic field profile as described above. To return the YBCO system to its initial state it was kept above room temperature for about one day. The resistance measurements have been performed under comparable conditions (see supplementary section S1).

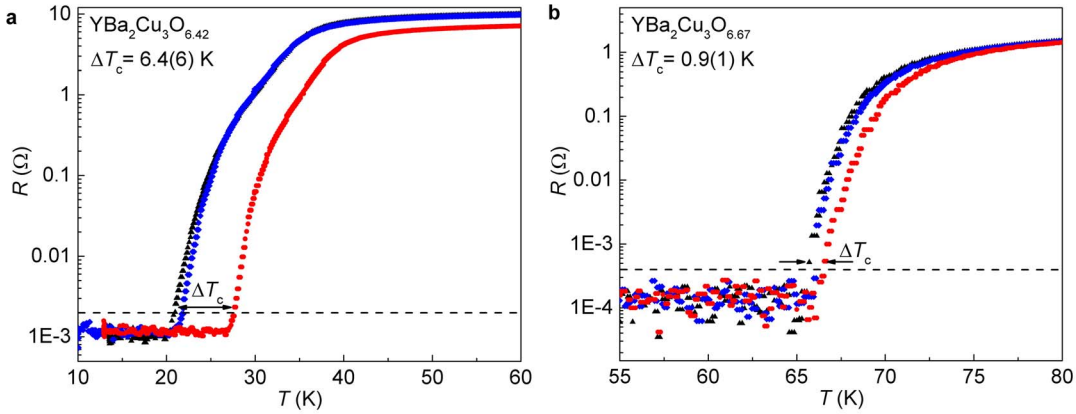

Figure 4 | Shifts in the critical temperature ΔT_c from resistance measurements. Resistance R versus temperature T of $YBa_2Cu_3O_{6.42}$ (**a**) and $YBa_2Cu_3O_{6.67}$ (**b**) thin films for the initial state (blue diamonds, before illumination), the illuminated state (red circles, after illumination at 270 K), and the recovered state (black triangles, sample kept above room temperature for about one day). The critical temperature T_c was determined as the temperature where R exceeds twice the RMS of the noise (dashed line) during heating of the samples. The shifts of the resistivity curves to lower values, after illumination at 270 K, reflect an increased charge carrier density at all temperatures $T < 270$ K. The arrows indicate the shifts in the transition temperatures ΔT_c due to visible-light illumination.

length over which the changes of n_s take place. The solution of this phenomenological model, used for fitting, is described in detail in the supplementary section S3. The estimated values of ζ obtained from the μSR data are of the order of the optical light penetration depth. Taking ellipsometry measurements of our thin film samples in the pristine state into account we find an average light penetration depth of $\zeta = 60(10)$ nm, consistent with previous studies on single crystals[27,28], as presented in the supplementary section S2. Hence, we used this value for the detailed analysis of $n_s(z)$.

The substantial changes of n_s due to illumination are more pronounced for strongly underdoped samples as observed in the thin film sets: The measured change of the superfluid density at the vacuum interface $n_{s,illum}/n_{s,0} = 1+(\lambda_I/\lambda_P)^2$ is much larger for $x = 0.42$ [$n_{s,illum}/n_{s,0} = 3.9(2)$] than for $x = 0.67$ [$n_{s,illum}/n_{s,0} = 1.45(3)$]. In all sample sets investigated the PPC is fully reversible. After the thermal reset, the original Meissner screening profile is recovered as depicted in Fig. 2.

Studies of single crystals were used to determine the role of disorder on the influence of the photo-induced changes. The investigated YBCO ortho-VIII single crystals consist of alternating Cu-O chains which are completely empty or full, forming a superstructure in the CuO_x layers[29]. Therefore, the amount of disorder is greatly reduced compared to our thin-film sample sets with equal doping level ($x = 0.67$). Moreover, the single crystals are detwinned which allows us to investigate the anisotropy of the photo-induced effect. Assuming pinned charge carriers along the c axis [scenario (ii)], photo-persistent effects comparable to those in the thin-film sets are expected. In the ortho-VIII single crystal mosaic, the superfluid density at the vacuum interface is increased [$n_{s,illum}/n_{s,0}$(ortho-VIII)$= 1.7(1)$] if the magnetic field is applied along the a axis (shielding currents flow along the Cu-O chains). The observation agrees with our thin-film results, implying that the Cu-O chains are also lengthened in less disordered single crystals due to illumination or showing that the order is not as perfect in the near-surface region compared to the bulk. The slightly larger effect in the single crystal mosaic compared to the thin-film set of equal doping could result from the 15% higher photon dose due to the longer illumination time (see supplementary table S1). When the magnetic field is applied parallel to the b axis no effect on $B(z)$ is observed. Within the experimental uncertainty the change of the superfluid density at the vacuum interface $n_{s,illum}/n_{s,0}$ has to be smaller than 1.06 for $B_{ext}||b$-axis.

The anisotropic PPC behaviour can be related to the in-plane anisotropy present in YBCO. The in-plane London penetration depths were determined as described in Refs. 18, 19 and found to be $\lambda_a = 177(5)$ nm ($B_{ext}||b$) and $\lambda_b = 158(2)$ nm ($B_{ext}||a$). The anisotropy between λ_a and λ_b is well known from optimally doped YBCO[18,30]. The ratio $\lambda_a/\lambda_b = 1.12(3)$ of the ortho-VIII single crystal set is only slightly smaller compared to the values of optimally doped YBCO determined by various methods (μSR: $\lambda_a/\lambda_b = 1.16$–$1.19$)[18], although it strongly depends on the doping level and the amount of oxygen disorder. The large in-plane anisotropy is discussed in the context of multiband effects[31]. This proximity model takes into account a contribution of the Cu-O chains to the superfluid density by assuming a hybridization of plane and chain wave functions within a three-band tight-binding Hamiltonian. Disorder within the Cu-O chains localizes a small fraction of the chain electron states, yielding a higher λ_b, but has no effect on λ_a[31]. Since the illumination of YBCO rearranges the Cu-O chains the amount of disorder within the Cu-O chains is reduced, thus diminishing the fraction of localized chain electrons. According to the proximity model, the additional superfluid density only affects λ_b, consistent with our experimental data (see Fig. 2c-d).

The presented LE-μSR data show a significant change in the magnetic penetration profile in the Meissner state of underdoped YBCO caused by an accumulated superfluid density n_s close to the surface. The persistent photo-induced changes of $n_s(z)$ appear only on a length scale comparable to the light penetration depth. The illumination stimulates a self-organization of the Cu-O chains in YBCO and hence reduces disorder. This may suggest that the reduced disorder leads to a non-trivial modification of the local band structure, probably due to hybridization of CuO_2 planes and chain layers, which in turn strengthens the superconducting ground state. Our results show the tremendous impact of nano-scale disorder on the superconducting ground state of cuprate superconductors.

Methods

Sample preparation and characterization. The $YBa_2Cu_3O_{6+x}$ (YBCO) thin films were deposited on single crystal 1×1 cm^2 (001) $SrTiO_3$ substrates by on-axis pulsed laser deposition from a stoichiometric target using a KrF excimer laser ($\lambda = 248$ nm). To grow YBCO layers with a thickness of 400(20) nm and 490(60) nm, 3000 and 4800 laser pulses with a laser repetition rate of 5 Hz were used under an oxygen partial pressure of 0.3 mbar. After deposition at 800°C, the samples were cooled to 780°C, where the chamber was flooded with 400 mbar oxygen to achieve fully oxidized films with a $T_c = 90.0(5)$ K. More details on the PLD growth are described in Refs. 32, 33. The layer thicknesses were determined by measuring the height of a chemical etched edge, ranging from the surface to the substrate, using atomic force microscopy. To check the homogeneity of the samples the thickness was measured at several points.

The reduction of the oxygen content was realized by a post-annealing process in a tubular furnace, described in detail in Ref. 34. In particular, the samples were annealed

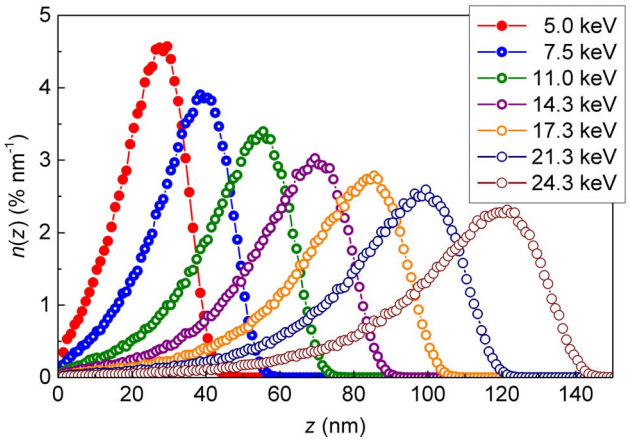

Figure 5 | Muon stopping profiles in YBCO. The normalized stopping distribution $n(z)$ for positively charged muons at different implantation energies for YBCO was simulated with TRIM.SP[38]. The lines are guides to the eye.

at a defined time and temperature in a flowing O_2/N_2 gas mixture. The process was concluded with a rapid cooling step to temperatures below 100°C in order to freeze in the oxygen concentration of the thin films. Annealing of the 400 nm thick samples at 450°C for 40 min in 2860 ppm O_2 atmosphere reduced the T_c of the YBCO to 66.7(8) K (corresponding to $x = 0.67$). The 490 nm thick films with $T_c = 21(2)$ K ($x = 0.42$) were annealed for 70 min at 500°C in a 215 ppm O_2 atmosphere. Purely c-axis oriented growth of YBCO was verified by $\Theta - 2\Theta$ measurements using a Bruker D8 Advance X-ray powder diffractometer with a Co anode. The resistivity measurements were performed with a four-point measurement on a cold finger cryostat in ultra high vacuum (about 10^{-8} mbar) under comparable conditions used for the μSR experiments.

The YBCO ortho-VIII single crystals were grown by the self-flux technique described in detail in Ref. 35. For the growth, $BaZrO_3$ ceramic crucibles were fabricated. After the self-flux growth the YBCO crystals were annealed in flowing oxygen for six days at 648°C, to set the oxygen content to $x = 0.67$. Afterwards the crystals were sealed in a quartz tube and annealed at 570°C for four days to homogenize the oxygen. During detwinning, the sample is heated to 180 – 250°C and squeezed with a pressure of about 100 MPa along one of the a/b axes under flowing nitrogen gas, causing the twin domains to reorient so that the a-axis (which has a shorter lattice constant) is along the direction of the pressure. For the formation of the oxygen vacancy ordered superstructure ortho-VIII, the YBCO single crystals were low temperature annealed at 40 – 42°C for five days. The final YBCO ortho-VIII single crystals had an estimated critical temperature of $T_c \simeq 66.5(5)$ K. One year later a $T_c = 67.8(5)$ K was determined with a Quantum Design MPMS SQUID magnetometer. The increase of T_c of about 1 K with time is natural in these crystals and is even expected, as the chain oxygen atoms slowly become better ordered even at room temperature and some of the interstitial oxygen impurities enter the Cu-O chains.

Low-energy muon spin rotation. The LE-μSR experiments were performed at the μE4 beamline at the Paul Scherrer Institut (PSI, Switzerland). For the thin-film measurements a mosaic of four 1×1 cm^2 large samples was glued with silver paint onto a nickel-coated aluminum plate. For the YBCO ortho-VIII measurements, a mosaic of 13 aligned single crystals, with an average size of about $2.1 \times 1.7 \times 0.2$ mm^3, was used. The measurements have been performed in ultra high vacuum (about 10^{-9} mbar) on a cold finger cryostat.

The μSR technique uses positively charged muons (μ^+) as a local magnetic probe. To investigate the magnetic penetration depth profile $B(z)$, the muons are slowed down using a solid Ar/N_2 moderator, so that they stop on a nm scale in condensed matter. At the μE4 beamline the low energy muons are produced at a rate of about 10^4 s^{-1} [16] with ~ 100% spin polarization[36]. The muons are implanted into the sample where they thermalize within a few picoseconds without noticeable loss of polarization. There they decay after a mean μ^+ lifetime of $\tau_\mu = 2.197$ μs into a positron (e^+) and two neutrinos ($\bar{\nu}_\mu$, ν_e):

$$\mu^+ \rightarrow e^+ + \bar{\nu}_\mu + \nu_e.$$

The positrons are preferentially emitted along the μ^+ spin direction at the time of decay due to the parity violation in the weak decay. Therefore, the detection of the time difference $t = t_e - t_s$ between the implantation time t_s and the decay time t_e of the μ^+ allows one to determine the temporal evolution of the muon-spin polarization $P(t)$ using the expression[37]:

$$N(t) = N_0\, e^{-t/\tau_\mu}[1 + AP(t)] + N_{Bkg}, \qquad (3)$$

where $N(t)$ is the number of decay positrons at time t. The scale of the counted positrons is given by N_0. A is the observable decay asymmetry and N_{Bkg} is a time-independent background of uncorrelated events. More details on the LE-μSR technique are given in Refs. 16, 17. The experiments were performed in the Meissner state. After zero field cooling to 5 K, a magnetic field $B_{ext}/\mu_0 < H_{c1}$ was applied parallel to the surface of the sample. The muon-spin polarization function $P(t)$ is then given by

$$P(t) = e^{-\sigma^2 t^2/2} \int n(z) \cos[\gamma_\mu B(z) t + \phi]\, dz, \qquad (4)$$

where ϕ is the initial angle of the muon spin direction relative to the positron detector. The gyromagnetic ratio of the muon is $\gamma_\mu = 2\pi \cdot 135.5$ MHz/T. The depolarization rate σ is a measure of any inhomogeneous local magnetic field distribution at the μ^+ stopping site. The muon stopping distributions $n(z)$ (see Fig. 5) were simulated for energies in the range 5 – 25 keV using the Monte Carlo code TRIM.SP[38]. The reliability of these simulations has been studied in various thin films[17,39]. The mean stopping depth $\bar{z} = \int n(z)\, z\, dz$ of the muons in YBCO is in the range 25 – 106 nm. The corresponding mean magnetic field is $\bar{B}(\bar{z}) = \int n(z)\, B(z)\, dz$. To analyse the data, the penetration profiles given in supplementary section S3 were used for $B(z)$. The penetration depths λ_L were determined from global fits with the μSR data analysis software package musrfit[40], where μSR spectra for different energies are analysed simultaneously.

See supplementary information for full details on the illumination conditions, the ellipsometry measurements, and the penetration profile model.

1. Kakalios, J. & Fritzsche, H. Persistent Photoconductivity in Doping-Modulated Amorphous Semiconductors. *Phys. Rev. Lett.* **53**, 1602 (1984).
2. Prokscha, T. *et al.* Photo-induced persistent inversion of germanium in a 200-nm-deep surface region. *Sci. Rep.* **3**, 2569 (2013).
3. Testardi, L. R. Destruction of Superconductivity by Laser Light. *Phys. Rev. B* **4**, 2189 (1971).
4. Fausti, D. *et al.* Light-induced Superconductivity in a Stripe-Ordered Cuprate. *Science* **331**, 189 (2011).
5. Kirilyuk, A. I., Kreines, N. M. & Kudinov, V. I. Frozen photoconductivity in YBaCuO films. *JETP Lett.* **52**, 49 (1990).
6. Kudinov, V. I., Kirilyuk, A. I. & Kreines, N. M. Photoinduced superconductivity in YBaCuO films. *Phys. Lett. A* **151**, 358 (1990).
7. Yu, G., Heeger, A. J., Stucky, G., Herron, N. & McCarron, E. M. Transient photoinduced conductivity in semiconducting single crystals of $YBa_2Cu_3O_{6.3}$: Search for photoinduced metallic state and for photoinduced superconductivity. *Solid State Commun.* **72**, 345-349 (1989).
8. Tanabe, K., Kubo, S., Hosseini Teherani, F., Asano, H. & Suzuki, M. Effects of Photoinduced Hole Doping on Normal-State and Superconducting Transport in Oxygen-Deficient $YBa_2Cu_3O_y$. *Phys. Rev. Lett.* **72**, 1537 (1994).
9. Kudinov, V. I. *et al.* Persistent photoconductivity in $YBa_2Cu_3O_{6+x}$ films as a method of photodoping toward metallic and superconducting phases. *Phys. Rev. B* **47**, 9017 (1993).
10. Veal, B. W. *et al.* Observation of temperature-dependent site disorder in $YBa_2Cu_3O_{7-\delta}$ below 150°C. *Phys. Rev. B* **42**, 6305 (1990).
11. Bubb, D. M. *et al.* Wavelength and photon dose dependence of infrared quenched persistent photoconductivity in $YBa_2Cu_3O_{6+x}$. *Phys. Rev. B* **60**, 6827 (1999).
12. Milić, M. M., Lazarov, N. Dj. & Cucić, D. A. Study on the photo-induced oxygen reordering in $YBa_2Cu_3O_{6+x}$. *Nucl. Inst. and Meth. in Phys. Res. B* **279**, 215-218 (2012).
13. Bubb, D. M. & Federici, J. F. Cellular automata model for persistent photoconductivity in YBCO. *J. Phys.: Condens. Matter* **12**, L261-L267 (2000).
14. Kula, W. & Sobolewski, R. Charging effect in partially oxygen-depleted superconducting Y-Ba-Cu-O thin films. *Phys. Rev. B* **49**, 6428(R) (1994).
15. Grigelionis, G., Tornau, E. E. & Rosengren, A. Effect of an electric field on oxygen ordering and superconducting temperature of $YBa_2Cu_3O_{6+x}$ thin films. *Phys. Rev. B* **53**, 425 (1996).
16. Prokscha, T. *et al.* The new μE4 beam at PSI: A hybrid-type large acceptance channel for the generation of a high intensity surface-muon beam. *Nucl. Instrum. Methods Phys. Res., Sect. A* **595**, 317 (2008).
17. Morenzoni, E., Prokscha, T., Suter, A., Luetkens, H. & Khasanov, R. Nano-scale thin film investigations with slow polarized muons. *J. Phys.: Condens. Matter* **16**, S4583 (2004).
18. Kiefl, R. F. *et al.* Direct measurement of the London penetration depth in $YBa_2Cu_3O_{6.92}$ using low-energy μSR. *Phys. Rev. B* **81**, 180502(R) (2010).
19. Jackson, T. J. *et al.* Depth-Resolved Profile of the Magnetic Field beneath the Surface of a Superconductor with a Few nm Resolution. *Phys. Rev. Lett.* **84**, 4958 (2000).
20. Stilp, E. *et al.* Modifications of the Meissner screening profile in $YBa_2Cu_3O_{7-\delta}$ thin films by gold nanoparticles. *Phys. Rev. B* **89**, 020510(R) (2014).
21. Morenzoni, E. *et al.* The Meissner effect in a strongly underdoped cuprate above its critical temperature. *Nat. Commun.* **2**, 272 (2011).
22. Wojek, B. M. *et al.* Magnetism, superconductivity, and coupling in cuprate heterostructures probed by low-energy muon-spin rotation. *Phys. Rev. B* **85**, 024505 (2012).

23. Suter, A. *et al.* Observation of nonexponential magnetic penetration profiles in the Meissner state: A manifestation of nonlocal effects in superconductors. *Phys. Rev. B* **72**, 024506 (2005).
24. Kozhevnikov, V. *et al.* Nonlocal effect and dimensions of Cooper pairs measured by low-energy muons and polarized neutrons in type-I superconductors. *Phys. Rev. B* **87**, 104508 (2013).
25. Romanenko, A. *et al.* Strong Meissner screening change in superconducting radio frequency cavities due to mild baking. *Appl. Phys. Lett.* **104**, 072601 (2014).
26. Sonier, Jeff, E., Brewer, Jess, H. & Kiefl, Robert, F. μSR studies of the vortex state in type-II superconductors. *Rev. Mod. Phys.* **72**, 769 (2000).
27. Kircher, J. *et al.* Anisotropy and oxygen-stoichiometry dependence of the dielectric tensor of $YBa_2Cu_3O_{7-\delta}$ ($0 \leq \delta \leq 1$). *Phys. Rev. B* **44**, 217 (1991).
28. Kotz, A. L. *et al.* Anisotropy of the optical dielectric function in the *ab* plane for $YBa_2Cu_3O_{7-\delta}$. *Phys. Rev. B* **45**, 2577(R) (1992).
29. Zimmermann, M. v. *et al* Oxygen-ordering superstructures in underdoped $YBa_2Cu_3O_{6+x}$ studied by hard x-ray diffraction. *Phys. Rev. B* **68**, 104515 (2003).
30. Basov, D. N. *et al.* In-Plane Anisotropy of the Penetration Depth in $YBa_2Cu_3O_{7-x}$ and $YBa_2Cu_4O_8$ Superconductors. *Phys. Rev. Lett.* **74**, 598 (1995).
31. Atkinson, W. A. Disorder and chain superconductivity in $YBa_2Cu_3O_{7-\delta}$. *Phys. Rev. B* **59**, 3377 (1999).
32. Hühne, R. *et al.* Preparation of coated conductor architectures on Ni composite tapes. *Supercond. Sci. Technol.* **20**, 709 (2007).
33. Kiessling, A. *et al.* Nanocolumns in $YBa_2Cu_3O_{7-x}$/$BaZrO_3$ quasi-multilayers: formation and influence on superconducting properties. *Supercond. Sci. Technol.* **24**, 055018 (2011).
34. Pahlke, P., Trommler, S., Holzapfel, B., Schultz, L. & Hühne, R. Dynamic variation of biaxal strain in optimally doped and underdoped YBa2Cu3O7- thin films. *J. Appl. Phys.* **113**, 123907 (2013).
35. Liang, R., Bonn, D. A. & Hardy, W. N. Growth of YBCO single crystals by the self-flux technique. *Philos. Mag.* **92**, 2563 (2012).
36. Morenzoni, E. *et al.* Generation of very slow polarized positive muons. *Phys. Rev. Lett.* **72**, 2793 (1994).
37. Yaouanc, A. & Dalmas de Reotier, P. *Muon Spin Rotation, Relaxation, and Resonance: Applications to Condensed Matter* (Oxford University Press, Oxford, 2011).
38. Eckstein, W. *Computer Simulation of Ion-Solid Interactions* (Springer, Berlin, 1991).
39. Morenzoni, E. *et al.* Implantation studies of keV positive muons in thin metallic layers. *Nucl. Instr. Meth. B* **192**, 254 (2002).
40. Suter, A. & Wojek, B. M. Musrfit: A Free Platform-Independent Framework for μSR Data Analysis. *Phys. Procedia* **30**, 69 (2012).

Acknowledgments

We gratefully acknowledge H.-P. Weber for his technical support. We are indebted to M. Döbeli for the RBS measurements, Ch. Wang for the help to perform the ellipsometry measurements and A. Boris for helpful discussion of the ellipsometry data. The LE-μSR experiments were carried out at the μE4 beamline at SμS, Paul Scherrer Institut, Switzerland. This work was partly supported by the Swiss National Science Foundation.

Author contributions

E.S., A.S. and T.P. proposed the idea, performed the resistivity and μSR measurements, analysed the data and wrote the paper. Z.S. and R.F.K. were involved in the μSR measurements. P.P. and R.H. prepared and characterized the YBCO thin films. J.C.B., R.L., W.N.H. and D.A.B. prepared and characterized the YBCO ortho VIII single crystals. C.B. analysed the ellipsometry data. E.S., A.S., T.P., Z.S., E.M., H.K., P.P., R.H., C.B., C.B., R.L., W.N.H., D.A.B. and R.F.K. discussed the results and contributed to the manuscript.

Additional information

Supplementary information accompanies this paper at http://www.nature.com/scientificreports

Competing financial interests: The authors declare no competing financial interests.

How to cite this article: Stilp, E. *et al.* Controlling the near-surface superfluid density in underdoped $YBa_2Cu_3O_{6+x}$ by photo-illumination. *Sci. Rep.* **4**, 6250; DOI:10.1038/srep06250 (2014).

This work is licensed under a Creative Commons Attribution-NonCommercial-NoDerivs 4.0 International License. The images or other third party material in this article are included in the article's Creative Commons license, unless indicated otherwise in the credit line; if the material is not included under the Creative Commons license, users will need to obtain permission from the license holder in order to reproduce the material. To view a copy of this license, visit http://creativecommons.org/licenses/by-nc-nd/4.0/